IEEJ Journal of Industry Applications
J-STAGE Advance published date : May 12, 2023
DOI : 10.1541/ieejjia.22008067

Paper

Safe High Stiffness Impedance Control for Series Elastic Actuators using Collocated Position Feedback

Razvan Andrei Budau Petrea*a) Non-member, Roberto Oboe* Member
Giulia Michieletto* Non-member

Physical human–robot interaction applications requiring safety and compliance characteristics usually employ mechanical devices such as series elastic actuators (SEAs). So far, impedance control schemes for SEAs have been investigated to overcome the limited displayable stiffness at the end point, represented by the stiffness of a physical spring, in a passive manner. SEAs usually mount two encoders on both the motor and load sides for position measurements. However, in several applications, the installation of a load-side encoder is not feasible from both cost and manufacturing perspectives. In this scenario, a Kalman Filter based on micro electro mechanical system accelerometers has been proposed for estimating the external force and load side quantities, without the need for load-side encoders. Herein, a novel impedance control scheme leveraging this approach is proposed to effectively overcome the stiffness of the physical spring while maintaining passivity at the end point. Compared with conventional load-side encoder-based impedance control schemes, the proposed control scheme presents comparable performance, as demonstrated by simulation and experimental results.

Keywords: Series elastic actuator (SEA), impedance control, acceleration-based control, Kalman Filter.

1. Introduction

Recent technological improvements allow robotic systems to physically interact with humans or external environments accurately and effectively, giving birth to new fields of research and engineering applications, such as rehabilitative, collaborative, and assistive robotics. Safety is by far the most crucial aspect in this context, demanding actuation systems capable of displaying compliant behavior, monitoring the interaction force, and full backdrivability.

Series elastic actuators (SEAs) are becoming widely adopted in these applications due to the compliance obtained through an elastic element connected between the actuator mass (motor-side mass) and the end effector (load-side mass). SEAs have many interesting properties, such as accurate force/torque sensing, shock absorption capabilities, and high frequency disturbance rejection[2][3]. More importantly, closed-loop control actions allow modulating the output impedance of the SEA to a desired level, ensuring active backdrivability within the control bandwidth of the device.

Impedance control, which aims at modulating the dynamic relationship between interaction forces and motions[4], should be able to achieve high stiffness as well as low stiffness actuation, depending on the application at hand.

The concept of passivity has become popular when coupled stability between the control system and the external environment is of interest. Passivity is a sufficient condition in this sense, since external environments and humans are usually considered passive. Vallery et al.[5] derived conservative passivity conditions for a velocity-sourced cascade control when rendering a pure spring. Tagliamonte et al.[6] extended these conditions for the Voigt body, the Maxwell body and zero impedance. Tosun et al.[7] further investigated these works providing less conservative conditions. Li et al.[8] achieved passivity for a variable stiffness impedance controller in interaction with humans during rehabilitation. Shardyko et al.[9] performed a passivity analysis for a positive torque feedback controller. Moreover, Lee et al.[10] highlighted the difference in assessing passivity at the load port and at the spring port, showing that the former approach results in a safer rendering of a higher stiffness. Calanca et al.[11][12] proposed a passivity-based adaptive controller, extended with a sliding mode robustification action for interaction with humans or external environments[13].

One of the most widely used impedance control schemes in literature is represented by a scheme consisting of an inner loop transmission force PD controller and an outer loop load-side position PD controller[14], referred to as basic impedance control (BIC), which has been effectively applied in wearable robots[15] and robots with elastic joints[16].

A major issue is generally represented by the possibility of rendering an arbitrarily high stiffness, which is limited by the stiffness of the physical spring of the device when passivity is desired. Few notable works have been able to overcome this limitation, such as the one by Lee et al.[17]. Calanca et al.[18] employed the BIC scheme in combination with load-side acceleration feedback (BIC-AF), proving this approach an effective method to render arbitrarily high stiffness val-

This paper is based on Reference[1], which was presented at the IPEC-Himeji 2022 Conference, ©2022 IEEJ.

a) Correspondence to: razvanandrei.budaupetrea@phd.unipd.it
* Department of Management and Engineering, University Of Padova
Stradella San Nicola 3, 36100, Vicenza, Italy

ues while maintaining passivity. However, this method relies on position measurements obtained from a load-side encoder and computes the load-side acceleration through double differentiation. In particular, when the desired impedance has viscoelastic characteristics, the triple differentiation of the encoder measurement is required. High noise arising from quantization effects, especially when using low-resolution encoders, can considerably limit the performances and cause instability, as will be shown with experimental tests later.

The design of effective controllers for SEAs have benefitted from adopting the two-mass system model to also include the dynamics of the load, in contrast to the original approach of Pratt in[2], where a single-mass model was used. SEAs can therefore be employed at their full potential, given the feedback information available through the load-side encoder. Despite the huge benefits brought by load-side encoders, the installation of high-resolution encoders is not a viable solution in many applications. The load-side encoder increases the overall cost of the device, especially high-resolution ones, and can be cumbersome on many wearable devices. A method to address this problem was recently proposed by Yokoyama et al.[19], where the load-side encoder is replaced by a MEMS accelerometer, which is more beneficial in terms of cost, size, and ease of installation. A Kalman Filter (KF) relying only on the motor-side encoder and the load-side MEMS accelerometer measurements is employed to accurately estimate load-side quantities and the external force, also when gravity affects the device. Besides the possibility of measuring gravity, the availability of the load acceleration through MEMS accelerometers can add significant value to the whole control system, as already shown in[13][20].

In this paper, a novel impedance control scheme for SEAs based on the KF presented in[19] is proposed, to further investigate the potentialities offered by these sensors compared to encoders when mounted on the load side. The controller is expressed as a state-feedback law, involving the positions and velocities of both the motor and load sides, and the external force. The structure and properties of the controller are initially presented by assuming the full state as available, for ease of tractability, although the controller is implemented in practice with the estimated state. Simulations and experimental results are performed to show that the proposed controller can render an arbitrarily high pure stiffness at the spring port in a passive way, showing results comparable to state-of-the-art techniques. The stability and robustness of the controller are also discussed. Lastly, it will be shown that theoretically it is possible with the proposed approach to render a Voigt model, i.e. a viscoelastic system, by updating the disturbance model in the KF to estimate the derivative of the external force.

In summary, the main contributions of the paper are:

- The design of a novel state-feedback impedance controller for SEAs, able to render an arbitrarily high stiffness, in a passive way, and it is robust with respect to modeling errors;
- The practical applicability of the proposed scheme through a MEMS accelerometer-based Kalman Filter, without employing the load-side encoder;

The paper is structured as follows: in Sec. 2 the SEA model and the MEMS-based KF[19] are introduced; in Sec. 3 the BIC and BIC-AF methods, used for comparison, are briefly resumed. The proposed feedback impedance control scheme is presented for full state availability. Sec. 4 presents the proposed controller based on the KF estimated variables, along with stability considerations and performance analysis. Sec. 6 and Sec. 7 report the simulations and experimental results, respectively. Lastly, Sec. 8 concludes the paper and highlights future research.

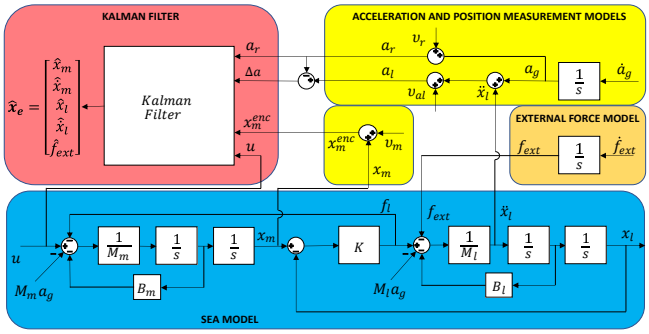

Figure 1 Block diagram of the linear SEA modeled through a two-mass system, acceleration and position measurements, external force model and Kalman Filter.

2. MEMS accelerometer-based Kalman Filter

This section briefly presents the SEA model and the KF employing two MEMS accelerometers presented in[19]. For simplicity, a linear SEA is considered throughout the paper since the same considerations can also be trivially extended for rotary SEAs.

2.1 SEA Model

SEAs can be modeled as two-mass systems, consisting of a motor-side mass which actuates the device, a load-side mass represented by the end effector, and an elastic component that connects the two masses. The dynamic equations are:

$$\begin{cases} f_m - f_s = M_m(\ddot{x}_m + a_g) + B_m\dot{x}_m \\ f_s = k(x_m - x_l) \\ f_s - f_{ext} = M_l(\ddot{x}_l + a_g) + B_l\dot{x}_l \end{cases} \quad \cdots\cdots\cdots\cdots (1)$$

where f_m is the actuator force, f_s is the transmission force of the elastic component, x_m and x_l are the motor-side and load-side positions, along with their first and second derivatives, M_m and M_l are the motor and the load masses, B_m and B_l are the motor and the load viscosities and k is the stiffness of the elastic component. f_{ext} is the external force acting on the load, which arises when the system is in contact with an external environment. a_g is the gravity acceleration, arising when the device is not placed parallel to the ground. The dependence of time is dropped for ease of readability. The corresponding block diagram is depicted in Fig. 1 (blue frame).

When the available measurements are the motor position x_m and the load acceleration $\ddot{x}_l$, since system (1) is linear and time-invariant, it can be expressed in the state-space domain as:

$$\begin{cases} \dot{\boldsymbol{x}} = \boldsymbol{A}\boldsymbol{x} + \boldsymbol{B}u + \boldsymbol{B_g}a_g + \boldsymbol{B_f}f_{ext} \\ \boldsymbol{y} = \boldsymbol{C}\boldsymbol{x} + \boldsymbol{D_g}a_g + \boldsymbol{D_f}f_{ext} \end{cases} \quad \cdots\cdots\cdots\cdots (2)$$

$$\boldsymbol{A} = \begin{bmatrix} -\frac{B_m}{M_m} & -\frac{k}{M_m} & 0 & \frac{k}{M_m} \\ 1 & 0 & 0 & 0 \\ 0 & \frac{k}{M_l} & -\frac{B_l}{M_l} & -\frac{k}{M_l} \\ 0 & 0 & 1 & 0 \end{bmatrix}$$

$$\boldsymbol{B} = \begin{bmatrix} \frac{1}{M_m} \\ 0 \\ 0 \\ 0 \end{bmatrix} \quad \boldsymbol{B_g} = \begin{bmatrix} -1 \\ 0 \\ -1 \\ 0 \end{bmatrix} \quad \boldsymbol{B_f} = \begin{bmatrix} 0 \\ 0 \\ -\frac{1}{M_l} \\ 0 \end{bmatrix}$$

$$\boldsymbol{C} = \begin{bmatrix} 0 & 1 & 0 & 0 \\ 0 & \frac{k}{M_l} & -\frac{B_l}{M_l} & -\frac{k}{M_l} \end{bmatrix} \quad \boldsymbol{D_g} = \begin{bmatrix} 0 \\ -1 \end{bmatrix} \quad \boldsymbol{D_f} = \begin{bmatrix} 0 \\ -\frac{1}{M_l} \end{bmatrix}$$

where $\boldsymbol{x} = [\dot{x}_m, x_m, \dot{x}_l, x_l]^T$, $\boldsymbol{y} = [x_m, \ddot{x}_l]^T$ and $u = f_m$. Therefore, the available SEA model can be considered as an SISO system with mismatched disturbances, represented by f_{ext} and a_g. Throughout this derivation, nonlinear effects, such as Coulomb friction, were neglected to address the problem by exploiting a linear input-output relation.

2.2 Kalman Filter When a load-side encoder cannot be mounted on the SEA device, a viable alternative is to install MEMS accelerometers on the device and employ state estimation techniques, such as the KF. Two MEMS accelerometers can be mounted on the support structure of the device and on the load, respectively. The support accelerometer serves for measuring only gravity, with measurement modeled as:

$$a_r = a_g + v_r \cdots\cdots (3)$$

where a_g is defined as in Sec. 2.1 and v_r represents measurement noise. The load-side acceleration measurement is modeled as:

$$a_l = \ddot{x}_l + a_g + v_{al} \cdots\cdots (4)$$

where v_{al} represents measurement noise. By combining (3) and (4), the load acceleration can be obtained as:

$$\Delta a = a_l - a_r = \ddot{x}_l + v_\Delta \cdots\cdots (5)$$

where $v_\Delta = v_{al} - v_r$ includes noise from both accelerometers. The motor-side encoder measurement is modeled as:

$$x_m^{enc} = x_m + v_m \cdots\cdots (6)$$

where v_m represents quantization noise of the sensor. All measurement models are depicted in Fig. 1 (yellow frames). The external force is directly comprised in the load acceleration due to the feedthrough matrix $\boldsymbol{D_f}$ in (2). It is possible to show that the external force is an observable state and can therefore be estimated. In this regard, a possible choice is to adopt a zero-order stochastic model:

$$\dot{f}_{ext} = w_{ext} \cdots\cdots (7)$$

where w_{ext} is a zero-mean Gaussian white noise, as depicted in Fig. 1 (orange frame).
Taking into account (1), (3), (4), (6) and (7) it is possible to define the augmented state-space model, updated with the measurement models, as:

$$\begin{cases} \dot{\hat{\boldsymbol{x}}}_e = \boldsymbol{A_e}\hat{\boldsymbol{x}}_e + \boldsymbol{B_e}\boldsymbol{u_e} + \boldsymbol{B_w}\boldsymbol{w} \\ \boldsymbol{y} = \boldsymbol{C_e}\hat{\boldsymbol{x}}_e + \boldsymbol{D_e}\boldsymbol{u_e} + \boldsymbol{v} \end{cases} \cdots\cdots (8)$$

$$\boldsymbol{A_e} = \begin{bmatrix} \boldsymbol{A} & \boldsymbol{B_f} \\ \boldsymbol{0} & 0 \end{bmatrix} \quad \boldsymbol{B_e} = \begin{bmatrix} \boldsymbol{B} & \boldsymbol{B_g} \\ 0 & 0 \end{bmatrix} \quad \boldsymbol{B_w} = \begin{bmatrix} \boldsymbol{B_e} & \boldsymbol{e_5} \end{bmatrix}$$

$$\boldsymbol{C_e} = \begin{bmatrix} \boldsymbol{C} & \boldsymbol{D_f} \\ \boldsymbol{0} & 0 \end{bmatrix} \quad \boldsymbol{D_e} = \begin{bmatrix} \boldsymbol{0} & \boldsymbol{D_g} \end{bmatrix}$$

where $\hat{\boldsymbol{x}}_e = \left[\dot{\hat{x}}_m, \hat{x}_m, \dot{\hat{x}}_l, \hat{x}_l, \hat{f}_{ext}\right]^T$, $\boldsymbol{y} = \left[x_m^{enc}, \Delta a\right]^T$, $\boldsymbol{u_e} = [f_m, a_g]^T$, $\boldsymbol{v} = [v_m, v_\Delta]^T$, and $\boldsymbol{w} = \left[w_p, w_g, w_{ext}\right]^T$. $\boldsymbol{e_5}$ is the fifth canonical base vector. The noises w_p, w_g, and w_{ext}, represent the process noise, the gravity acceleration noise, and the external force zero-mean Gaussian white noise. Subsequently, a KF is constructed to estimate the state of the augmented system $\hat{\boldsymbol{x}}$, as in Fig. 1 (red frame).
For details of the derivation of (8) and the implementation of the KF, the reader is referred to the original article[19], where a version without the support accelerometer is also discussed.
Remark 1 Higher-order models can be employed to estimate also the derivatives of the external force[21]. A first-order model will be applied in the implementation of the impedance controller when the desired impedance is represented by a Voigt model, which requires the first derivative of the external force.

3. Impedance Control Schemes

Various impedance control schemes have been proposed for SEAs. In the following, the proposed scheme is presented, involving a state feedback matrix and an external force feedback term. Only the case of a constant null reference $X_{lr}(s) = 0$ is considered, for the sake of simplicity. First, a brief recall is made for BIC[14] and BIC-AF[18].
Impedance control is used in tasks involving the interaction between the compliant motion of positioning devices and an external environment[22]. The impedance $I_L(s)$ is defined as the relationship between the external force and the load velocity, expressed in the Laplace domain, as:

$$I_L(s) = -\frac{F_{ext}(s)}{\dot{X}_l(s)}.$$

where the rendered impedance is considered at the load port[17]. Impedance controllers are instead frequently designed to render the desired relation at the spring port, which presents an impedance expressed as:

$$I_S(s) = -\frac{F_s(s)}{\dot{X}_l(s)}.$$

This choice is made since the impedance at the load port can be trivially extended by adding the load dynamics $G_l(s)$, as:

$$I_L(s) = I_S(s) + G_l(s)^{-1}.$$

For the derivation of the controller, the analysis will focus on rendering a pure spring of desired stiffness k_{des}, and a Voigt model which includes also a desired damping b_{des}. The impedance relations are therefore expressed as:

$$I_k(s) = \frac{k_{des}}{s} \qquad I_V(s) = \frac{k_{des}}{s} + b_{des}.$$

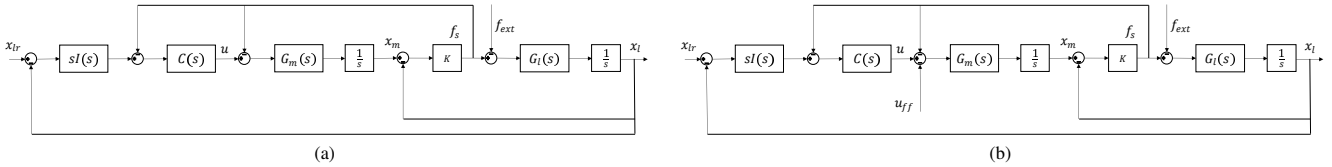

(a) (b)

Figure 2 Conventional controllers block diagrams: (a) BIC and (b) BIC-AF.

In the following, when using PD controllers in the considered schemes, the low-pass filtering of the derivative term is ignored for simplicity, resulting in:

$$C(s) = \Lambda_P + \Lambda_D s.$$

3.1 Basic Impedance Control The block diagram of the BIC scheme is depicted in Fig. 2(a), where the motor dynamics and the load dynamics, derived from (1), are grouped as:

$$G_m(s) = \frac{1}{M_m s + B_m} \qquad G_l(s) = \frac{1}{M_l s + B_l}.$$

This scheme employs an inner transmission force PD control loop and an outer non-collocated, load-side position loop to shape the impedance relation. By considering the desired impedance relation $I(s)$, which can be equal to the pure spring $I_k(s)$ or the Voigt model $I_V(s)$, the resulting rendered impedance $I_{res}(s)$ at the load port becomes:

$$I_{res}(s) = k\frac{C(s)I(s) + G_m^{-1}(s)}{sG_m^{-1}(s) + k(C(s)+1)} + G_l^{-1}(s) \cdots\cdots (9)$$

Passivity is usually used to ensure coupled stability, requiring $I_{res}(j\omega)$ to be stable and $\Re\big(I_{res}(j\omega)\big)$ to be positive. It is well known that a conservative condition which assures passivity is represented by $k_{des} \leq k$. The load viscosity B_l, however, allows to slightly increase this upper limit[10].

3.2 BIC with Acceleration Feedback The BIC-AF scheme, shown in Fig. 2(b), employs the control scheme reported in Sec. 3.1 and adds a term u_{ff} which depends on the load acceleration. The resulting impedance relation at the load port becomes:

$$I_{res}(s) = k\frac{C(s)I(s) + G_m^{-1}(s) + u_{ff}(s)}{sG_m^{-1}(s) + k(C(s)+1)} + G_l^{-1}(s). (10)$$

By choosing u_{ff} as:

$$u_{ff}(s) = \left(\frac{G_m^{-1}(s)}{s}\left(\frac{sI(s)}{k} - 1\right) + \frac{I(s)}{s}\right)\ddot{X}_l(s) \cdots (11)$$

the resulting impedance at the spring port becomes equal to the desired one, leading to:

$$I_{res}(s) = I(s) + G_l^{-1}(s)$$

which is trivially passive for any value of k_{des} since it is stable and $\Re\big(I_{res}(j\omega)\big) = B_l$.
However, it is worth noting that for $I(s) = I_k(s)$ antitransforming (11) leads to:

$$u_{ff} = M_m\left(\frac{k_{des}}{k} - 1\right)\ddot{x}_l + B_m\left(\frac{k_{des}}{k} - 1\right)\dot{x}_l + k_{des}x_l \cdot (12)$$

implying that not only the load-side acceleration is fed back into the system, but also terms depending on the velocity and the position are involved.

Remark 2 In the original proposed BIC-AF, the damping term B_m was not considered in the motor-side equations, leading to the absence of the velocity-dependent term in (12). This choice is not inconsistent, since the impedance at the spring port in this case becomes:

$$I_{res}(s) = I(s)\frac{M_m s^2 + (B_m\frac{k}{k_{des}} + \Lambda_D k)s + k(1+\Lambda_P)}{M_m s^2 + (B_m + \Lambda_D k)s + k(1+\Lambda_P)} + G_l^{-1}(s)$$

where the term multiplying $I(s)$ is equal to 1 at almost all frequencies and does not compromise the impedance rendering. This consideration seems to allow one to design an effective controller without the need to accurately identify the motor viscosity B_m. However, checking the passivity condition, it follows:

$$\begin{aligned}
&\Re\big(I_{res}(j\omega)\big) = B_m\frac{a_1\omega^2 + a_2}{M_m^2\omega^4 + b_1\omega^2 + b_2}\\
&a_1 = M_m(k_{des} - k)\\
&a_2 = k(k - k_{des})(1+\Lambda_P)\\
&b_1 = (B_m + k\Lambda_D)^2 + 2k(B_m\Lambda_D - M_m(1+\Lambda_P))\\
&b_2 = k^2(1+\Lambda_P)^2
\end{aligned}$$

which highlights the non-triviality of ensuring passivity and compromises the possibility of rendering an arbitrarily high virtual stiffness.
For the $I_V(s)$ case, by antitransforming (11), the following feedback term is obtained:

$$\begin{aligned}
u_{ff} = \ & \tfrac{1}{k}\Big(M_m b_{des}\dddot{x}_l + \\
& + (B_m b_{des} + M_m(k_{des} - k))\ddot{x}_l + \\
& + \big(k b_{des} + B_m(k_{des} - k)\big)\dot{x}_l + k k_{des} x_l\Big)
\end{aligned} \qquad (13)$$

which also depends on the load jerk $\dddot{x}_l$.
The original proposed BIC-AF used a load encoder to measure x_l and obtained all derivative terms through differentiation of the measurement. It is well known that this operation introduces high frequency noise and therefore represents a significant limitation, especially for the Voigt model case.

3.3 State and External Force Feedback Control The proposed scheme based on state and external force feedback (SEFF) is illustrated in Fig. 3(a), consisting of a static state-feedback matrix $\boldsymbol{K_x}$, and a proportional feedback gain from the external force, K_f. The controller is initially derived by considering the desired impedance as $I_k(s)$.
Exploiting (2), and assuming the full state and the external force as available, the equations of the system with the proposed control law are:

$$\begin{cases}
\dot{\boldsymbol{x}} = \boldsymbol{A}\boldsymbol{x} + \boldsymbol{B}u + \boldsymbol{B_f}f_{ext}\\
\boldsymbol{y} = \boldsymbol{x_e}\\
u = -\begin{bmatrix}\boldsymbol{K_x} & K_f\end{bmatrix}\begin{bmatrix}\boldsymbol{x}\\ f_{ext}\end{bmatrix} = -\boldsymbol{K_e}\boldsymbol{x_e}
\end{cases} \cdots\cdots\cdots (14)$$

where:

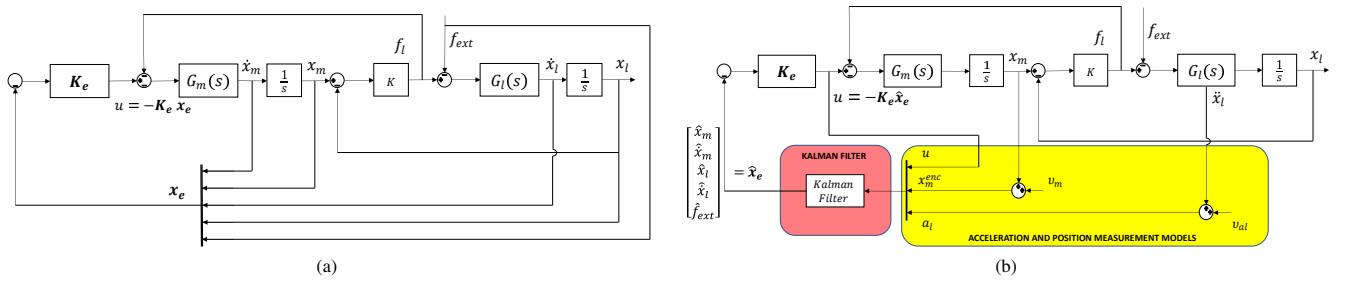

Figure 3 Proposed controller SEFF block diagrams: (a) full-state and external force availability and (b) KF-estimated variables.

$$\begin{cases} \boldsymbol{K_x} = \begin{bmatrix} \Lambda_{D_m} & \Lambda_{P_m} & \Lambda_{D_l} & \Lambda_{P_l} \end{bmatrix} \\ \Lambda_{D_m} = D \\ \Lambda_{P_m} = P + \frac{M_m}{M_l}(k_{des} - k) \\ \Lambda_{D_l} = \left(\frac{k_{des}}{k} - 1\right)\left(D + B_m - \frac{M_m}{M_l}B_l\right) \\ \Lambda_{P_l} = k_{des} + \left(\frac{k_{des}}{k} - 1\right)\left(P - \frac{kM_m}{M_l}\right) \\ K_f = \Lambda_f = \frac{M_m}{M_l}\left(\frac{k_{des}}{k} - 1\right) \end{cases} \cdots\cdots\cdots (15)$$

P and D have the same role as the parameters Λ_P and Λ_D in the PD controllers from the previous subsections.
To understand the design of the controller, consider the relation from f_{ext} to $\dot{x}_l$ from (1) (neglecting gravity) when $u = -\boldsymbol{K_e x_e}$ where the elements of $\boldsymbol{K_e}$ are generic. This leads to:

$$\begin{aligned} F_{ext}(s) &= \frac{N_f(s)}{D_f(s)} \\ N_f(s) &= -(M_l s^2 + B_l s + k)(M_m s^2 + (\Lambda_{D_m} + B_m)s + \Lambda_{P_m} + k) \\ &\quad - k(\Lambda_{P_l} - k + \Lambda_{D_l} s) \\ D_f(s) &= s(M_m s^2 + (\Lambda_{D_m} + B_m)s + \Lambda_{P_m} + k + \Lambda_f k) \end{aligned}$$

From this relation it can be easily be noted that Λ_{D_m}, Λ_{P_m} only act on modifying the motor-side dynamics (present both in $N_f(s)$ and $D_f(s)$), Λ_{D_l}, Λ_{P_l} on the load-side dynamics (present in $N_f(s)$), while Λ_f acts in a feedback fashion, allowing to modulate even further $D_f(s)$. By comparison, it is possible to design $\boldsymbol{K_e}$ with the values in (15) for modifying the output impedance.
After applying the control law in (14) to the system, the resulting system can be rearranged as:

$$\begin{cases} \dot{\boldsymbol{x}} = \boldsymbol{Ax} - \boldsymbol{B}\begin{bmatrix} \boldsymbol{K_x x} & K_f f_{ext} \end{bmatrix} + \boldsymbol{B_f} f_{ext} \\ \quad = (\boldsymbol{A} - \boldsymbol{BK_x})\boldsymbol{x} + (\boldsymbol{B_f} - \boldsymbol{B}K_f) f_{ext} \\ \quad = \boldsymbol{A_{cl}x} + \boldsymbol{B_{cl}} f_{ext} \\ \boldsymbol{W}_{cl}(s) = (s\boldsymbol{I} - \boldsymbol{A_{cl}})^{-1}\boldsymbol{B_{cl}}. \end{cases} \cdots (16)$$

The first equation in (16) represents the closed-loop relation, i.e. a system described by the matrices $(\boldsymbol{A_{cl}}, \boldsymbol{B_{cl}})$ commanded by the external force acting as the only input. This relation can be used for stability analysis by checking the four eigenvalues λ_i of $\boldsymbol{A_{cl}}$:

$$\begin{cases} \lambda_{1,2} = \dfrac{-(B_m + D) \pm \sqrt{(B_m + D)^2 - 4M_m(P + K)}}{2M_m} \\ \lambda_{3,4} = \dfrac{-B_l \pm \sqrt{B_l^2 - 4k_{des}M_l}}{2M_l}. \end{cases}$$

From $\lambda_{1,2}$ it is clear that an appropriate tuning must be performed on P and D to stabilize the system and regulate the performances.
From $\lambda_{3,4}$ it is clear that when k_{des} is sufficiently high ($k_{des} > \frac{B_l^2}{4M_l}$), it does not affect the real part of the eigenvalues, which is always negative and equal to $\frac{-B_l}{2M_l}$. Conversely, if k_{des} is sufficiently small ($k_{des} \leq \frac{B_l^2}{4M_l}$), the real part of λ_3 increases, becoming null in the limit case $k_{des} = 0$.
The second equation in (16) is the resulting transfer function matrix from the external force to the states. From the third element of $\boldsymbol{W}_{cl}(s)$, which relates f_{ext} and $\dot{x}_l$, the rendered impedance at the load port can be obtained, which is:

$$I_{res}(s) = \frac{k_{des}}{s} + G_l^{-1}(s)$$

thus rendering an impedance with arbitrary stiffness in a passive way, as obtained also with the BIC-AF. In fact, it is possible to prove that by selecting the PD parameters for the BIC-AF case as $\Lambda_P = P/k$, $\Lambda_D = D/k$, the resulting control action is equal to the proposed one. The main difference between the two schemes is in how the information is acquired and processed: the BIC-AF uses the load acceleration, whereas the proposed scheme uses the external force. Moreover, in practical implementations, the BIC-AF relies on the load-side encoder signal and its differentiation. In contrast, the proposed scheme needs the external force measurement, which is rarely available in this context. Despite this seeming a drawback, many SEA control schemes are implemented using observer-based techniques for external force estimation and feedback. Regarding the case $I_V(s)$, similar considerations can be made as for the pure spring case, and will not be reported here for ease of tractation. The discussion is limited to providing the control law, which is:

$$\begin{cases} u = -\boldsymbol{K_e x_e} - \Lambda_{P_{l_2}} x_l - \Lambda_{D_{l_2}} \dot{x}_l \\ \quad - \Lambda_{f_2} f_{ext} - \Lambda_{df} \dot{f}_{ext} \\ \Lambda_{P_{l_2}} = \dfrac{k_{des}}{kM_l^2}(B_l - b_{des})\left(M_l(B_m + D) - M_m b_{des}\right) \\ \Lambda_{D_{l_2}} = \dfrac{(B_l - b_{des})}{kM_l^2}\left(M_m b_{des}^2 + M_l^2(k + P)\right. \\ \quad \left. - M_l(b_{des}(B_m + D) + M_m k_{des})\right) \\ \Lambda_{f_2} = \dfrac{(B_l - b_{des})}{kM_l^2}\left(M_l(B_m + D) - M_m b_{des}\right) \\ \Lambda_{df} = \dfrac{M_m}{kM_l}(B_l - b_{des}) \end{cases} \quad (17)$$

Compared to the pure stiffness case, this control law adds other feedback terms depending on the load position, load

velocity, the external force and its derivative.

Remark 3 For the practical implementation, the external force and its first derivative can be obtained by employing, as stated in Sec. 2.2, a first-order model in the KF:

$$\dddot{f}_{ext} = w_{ext}.$$

4. KF-based State and External Force Feedback Control

When the KF presented in Sec. 2.2 is applied in synergy with the proposed SEFF controller, the resulting block diagram becomes the one illustrated in Fig. 3(b), where the influence of gravity is neglected for a fair comparison with the other methods. Here, only the case $I(s) = I_k(s)$ is considered, for simplicity. The measured load acceleration, the measured motor position, and the input are fed into the KF to produce the estimated augmented state $\hat{\boldsymbol{x}}_e$, which is then applied in the feedback control law. The equations of the system become:

$$\begin{cases} \dot{\boldsymbol{x}} = \boldsymbol{A}\boldsymbol{x} + \boldsymbol{B}u + \boldsymbol{B_f} f_{ext} \\ \boldsymbol{y} = \boldsymbol{C}\boldsymbol{x} + \boldsymbol{D}_f f_{ext} \\ u = -\begin{bmatrix} \boldsymbol{K_x} & K_f \end{bmatrix} \begin{bmatrix} \hat{\boldsymbol{x}} \\ \hat{f}_{ext} \end{bmatrix} = -\boldsymbol{K_e}\hat{\boldsymbol{x}}_{\boldsymbol{e}} \quad \cdots\cdots\cdots (18) \\ \dot{\hat{\boldsymbol{x}}}_e = \boldsymbol{A_e}\hat{\boldsymbol{x}}_{\boldsymbol{e}} + \boldsymbol{B_e}u + \boldsymbol{L}(\boldsymbol{y} - \hat{\boldsymbol{y}}) \\ \hat{\boldsymbol{y}} = \boldsymbol{C_e}\hat{\boldsymbol{x}}_e \end{cases}$$

where the last two equations represent the dynamic system of the KF. $\boldsymbol{L}$ is the steady-state Kalman gain, and the other matrices are the same as defined in Sec. 2.2.

By splitting the Kalman gain as $\boldsymbol{L} = [\boldsymbol{L_1}, \boldsymbol{L_2}]$ and defining the estimation errors $\boldsymbol{e} = [\boldsymbol{e}_x, e_f]^T = [\boldsymbol{x} - \hat{\boldsymbol{x}}, f_{ext} - \hat{f}_{ext}]^T$ the dynamic equations for the estimation error can be straightforwardly computed as:

$$\begin{bmatrix} \dot{\boldsymbol{e}}_x \\ \dot{e}_f \end{bmatrix} = \begin{bmatrix} \boldsymbol{A} - \boldsymbol{L_1}\boldsymbol{C} & \boldsymbol{B_f} \\ \boldsymbol{0} & \boldsymbol{L_2}\boldsymbol{D_f} \end{bmatrix} \begin{bmatrix} \boldsymbol{e}_x \\ e_f \end{bmatrix} \quad \cdots\cdots\cdots\cdots (19)$$

meaning that an appropriate design of $\boldsymbol{L}$ results in a stable observer and convergence of the estimation error.

In the same way, the dynamic equations for the true system can be rewritten as:

$$\begin{bmatrix} \dot{\boldsymbol{x}} \\ \dot{f}_{ext} \end{bmatrix} = \begin{bmatrix} \boldsymbol{A} & \boldsymbol{B_f} \\ \boldsymbol{0} & 0 \end{bmatrix} \begin{bmatrix} \boldsymbol{x} \\ f_{ext} \end{bmatrix} - \begin{bmatrix} \boldsymbol{B}\boldsymbol{K_x} & \boldsymbol{B}K_f \\ 0 & 0 \end{bmatrix} \begin{bmatrix} \hat{\boldsymbol{x}} \\ \hat{f}_{ext} \end{bmatrix} \quad (20)$$

Using the relation $\hat{\boldsymbol{x}}_{\boldsymbol{e}} = [\boldsymbol{x} - \boldsymbol{e}_{\boldsymbol{x}}, f_{ext} - e_f]^T$, (20) can be rearranged as:

$$\begin{bmatrix} \dot{\boldsymbol{x}} \\ \dot{f}_{ext} \end{bmatrix} = \begin{bmatrix} \boldsymbol{A} - \boldsymbol{B}\boldsymbol{K_x} & \boldsymbol{B_f} - \boldsymbol{B}K_x \\ \boldsymbol{0} & 0 \end{bmatrix} \begin{bmatrix} \boldsymbol{x} \\ f_{ext} \end{bmatrix} + \boldsymbol{B}\boldsymbol{u_{err}}$$

where $\boldsymbol{u_{err}} = \boldsymbol{K_e}\boldsymbol{e}^T$. This expression highlights how the true system results in the sum of the system (16), augmented to include also f_{ext}, obtained by applying the control law (14) with a disturbance term depending on the estimation error.

Performances can therefore be analyzed as a function of $\boldsymbol{u_{err}}$, by deriving the transfer functions from each estimated error to $\dot{x}_l$. This leads to:

$$\frac{\dot{X}_l(s)}{\boldsymbol{E}(s)} = \frac{\begin{bmatrix} DkM_l \\ k\big(M_m(k_{des} - k) + M_l P\big) \\ (k - k_{des})\big(M_l(B_m + D) - M_m B_l\big) \\ (k - k_{des})(M_l P - M_m k) + M_l k k_{des} \\ M_m(k - k_{des}) \end{bmatrix}^T}{M_l\big(M_m s^2 + (B_m + D)s + k + P\big) I_k(s)}$$

These equations allow the designer to tune the parameters P and D to obtain the desired level of disturbance rejection, e.g. as a function of the expected maximum magnitude of each error term in $\boldsymbol{e}_x$.

5. Model Errors

In this section, the problem of modeling errors is considered and analyzed, in terms of stability of the closed loop and passivity. Since the controller requires all the system parameters to be designed, multiplicative parameter errors are considered on all variables, as:

$$\Delta_{M_m} > 0,\ \Delta_{M_l} > 0,\ \Delta_{B_m} > 0,\ \Delta_{B_l} > 0,\ \Delta_k > 0.$$

The controller (15) is then assumed to be implemented with parameters:

$$M_m\Delta_{M_m},\ M_l\Delta_{M_l},\ B_m\Delta_{B_m},\ B_l\Delta_{B_l},\ k\Delta_k,$$

with the objective of understanding how to tune P and D to meet the above-mentioned requirements. For simplicity, only the pure spring case is presented.

5.1 Passivity

For passivity, the impedance transfer function needs to be stable, and its real part must be positive for all frequencies ω. With modeling errors, the impedance relationship becomes:

$$\begin{aligned} I_\Delta(s) &= B_l + M_l s + \tfrac{N_I(s)}{D_I(s)} \\ N_\Delta(s) &= s^2 M_l M_m(\Delta_{M_m} k_{des} - \Delta_k\Delta_{M_m} k + \Delta_k\Delta_{M_l} k) \\ &\quad + s\big(B_m\Delta_{M_l} M_l(\Delta_{B_m} k_{des} + \Delta_k k - \Delta_k\Delta_{B_m} k) \\ &\quad + \Delta_{M_l} D M_l k_{des} - B_l\Delta_{M_m} M_m(\Delta_{B_l} - 1)(k_{des} - \Delta_k k)\big) \\ &\quad + \Delta_{M_l} M_l k_{des}(P + \Delta_k k) \\ D_\Delta(s) &= s^3 + \Delta_k\Delta_{M_l} M_l M_m + s^2\Delta_k\Delta_{M_l} M_l(D + B_m) \\ &\quad + s\big(\Delta_k\Delta_{M_l} M_l(P + k) + \Delta_{M_m} M_m(\Delta_k - 1)(k_{des} - \Delta_k k)\big) \end{aligned}$$

which is stable with the following condition, derived from $D_\Delta(s)$:

$$P > -k - \tfrac{\Delta_{M_m} M_m}{\Delta_k\Delta_{M_l} M_l}(\Delta_k - 1)(k_{des} - \Delta_k k) \cdots\cdots (21)$$

By assuming to choose $\Delta_k > 1$, meaning that the spring stiffness is overestimated, this condition highlights the necessity to increase P when small stiffness values are desired.

The real part of the frequency response can be derived with some calculations as:

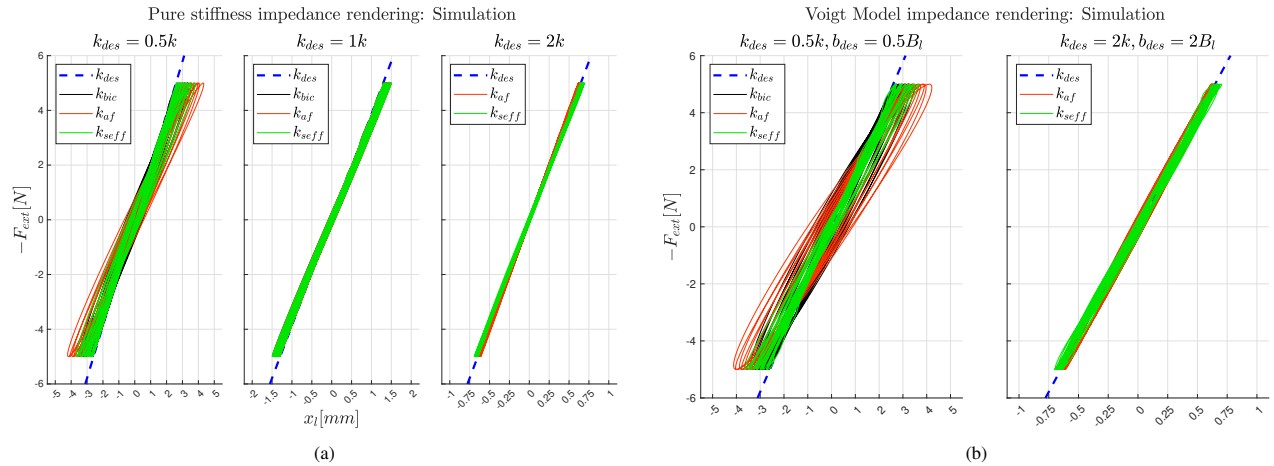

(a) (b)

Figure 4 Simulation results: (a) for pure spring $k_{des} = 0.5k, k, 2k$ and (b) Voigt model for $k_{des} = 0.5k$, $b_{des} = 0.5B_l$ and $k_{des} = 2k$, $b_{des} = 2B_l$. In all figures, dashed blue line is the desired stiffness, black line refers to BIC, red line refers to BIC-AF and green line refers to SEFF methods.

$$\Re\{I_\Delta(j\omega)\} = \frac{N_I(j\omega)}{D_I(j\omega)} = \frac{A_n\omega^4+B_n\omega^2+C_n}{(A_d\omega^2-B_d)^2+C_d\omega^2}$$

$$A_n = B_l{\Delta_k}^2{\Delta_{M_l}}^2{M_l}^2{M_m}^2$$

$$\begin{aligned}B_n = {} & B_l{\Delta_k}^2{\Delta_{M_l}}^2{M_l}^2(D+B_m)^2 \\ & + \Delta_k\Delta_{M_l}{M_l}^2M_m\big(B_m(\Delta_{M_m}-\Delta_{B_m}\Delta_{M_l}) \\ & - D(\Delta_{M_l}-\Delta_{M_m})\big)(k_{des}-\Delta_k k) \\ & - 2B_l{\Delta_k}^2{\Delta_{M_l}}^2{M_l}^2M_m(P+k) \\ & + B_l\Delta_k\Delta_{M_l}\Delta_{M_m}M_l{M_m}^2(k_{des}-\Delta_k k)(1+\Delta_{B_l}-2\Delta_k)\end{aligned}$$

$$\begin{aligned}C_n = {} & B_l\Big(\Delta_k k\big(\Delta_{M_l}M_l-\Delta_{M_m}M_m(\Delta_k-1)\big) \\ & + \Delta_{M_m}M_m k_{des}(\Delta_k-1)\Big)\Big(\Delta_k k\big(\Delta_{M_l}M_l \\ & - \Delta_{M_m}M_m(\Delta_k-\Delta_{B_l})\big)+\Delta_{M_m}M_m k_{des}(\Delta_k-\Delta_{B_l})\Big) \\ & + B_l{\Delta_k}^2{\Delta_{M_l}}^2P^2{M_l}^2-\Delta_k\Delta_{M_l}PM_l\Big(\big(B_m\Delta_{M_l}M_l \\ & + B_l\Delta_{M_m}M_m(1+\Delta_{B_l}-2\Delta_k)\big)(k_{des}-\Delta_k k) \\ & - \Delta_{M_l}M_l\big(2B_l\Delta_k k+B_m\Delta_{B_m}(k_{des}-\Delta_k k)\big)\Big) \\ & + B_m\Delta_{M_l}M_l(\Delta_{M_m}M_m(\Delta_k-1)(k_{des}-\Delta_k k) \\ & + \Delta_k\Delta_{M_l}M_l k)(\Delta_{B_m}-1)(k_{des}-\Delta_k k) \\ & - \Delta_{M_l}M_l k_{des}(\Delta_k-1)(D+B_m)(-\Delta_{M_m}M_m k_{des} \\ & + \Delta_k\Delta_{M_m}M_m k+\Delta_k\Delta_{M_l}M_l k)\end{aligned}$$

$$A_d = \Delta_k\Delta_{M_l}M_lM_m$$

$$B_d = \Delta_k\Delta_{M_l}M_l(P+k)+\Delta_{M_m}M_m(\Delta_k-1)(k_{des}-\Delta_k k)$$

$$C_d = {\Delta_k}^2{\Delta_{M_l}}^2{M_l}^2(D+B_m)^2.$$

The denominator is always positive, while the numerator is a fourth-order symmetric polynomial which can be studied by calculating its stationary point and deriving the conditions to ensure that it is positive. The derivative of $N_I(j\omega)$ is calculated and equaled to zero, obtaining:

$$\begin{cases}\omega_m = \Big(\frac{1}{2\Delta_k\Delta_{M_l}B_lM_lM_m^2}\Big(-2B_l\Delta_k\Delta_{M_l}PM_lM_m \\ \quad - B_lM_m\big(\Delta_{M_m}M_m(k_{des}-\Delta_k k)(1+\Delta_{B_l}-2\Delta_k) \\ \quad - 2\Delta_k\Delta_{M_l}M_lk\big)+M_lM_m\big(B_m(\Delta_{M_m}-\Delta_{B_m}\Delta_{M_l}) \\ \quad - D(\Delta_{M_l}-\Delta_{M_m})\big)(k_{des}-\Delta_k k) \\ \quad + B_l\Delta_k\Delta_{M_l}M_l(D+B_m)^2\Big)\Big)^{\frac{1}{2}} \\ P_\omega = P > \frac{1}{2B_l\Delta_k\Delta_{Ml}M_lM_m}\Big(M_m(k_{des}-\Delta_k k)(B_mM_l(\Delta_{M_m} \\ \quad - \Delta_{B_m}\Delta_{M_l})-DM_l(-\Delta_{M_m}+\Delta_{M_l})+B_l\Delta_{M_m}M_m(1 \\ \quad + \Delta_{B_l}-2\Delta_k))+B_l\Delta_k\Delta_{M_l}M_l(D+B_m)^2\Big)-k\end{cases} \tag{22}$$

When the condition P_ω is respected, similarly to (21), the stationary point exists and it is positive. By substituting (22) into $N_I(j\omega)$, with P greater than the value in P_ω by a positive value u, it follows:

$$\begin{aligned}N_I(j\omega_m) = {} & B_l{}^2\Delta_k{}^2\Delta_{M_l}{}^2M_l{}^2(D+B_m)^4 \\ & - 2B_l\Delta_k\Delta_{M_l}M_l{}^2M_m(\Delta_{M_l}-\Delta_{M_m})(k_{des} \\ & - \Delta_k k)(D+B_m)^3+2M_mM_l(D+B_m)f(u) \\ & - M_m(k_{des}-\Delta_k k)\Big(M_l{}^2M_m(k_{des}-\Delta_k k)(\Delta_{M_m}D \\ & - \Delta_{M_l}D+B_m\Delta_{M_m}-B_m\Delta_{B_m}\Delta_{M_l})^2 \\ & + B_l{}^2\Delta_{M_m}{}^2M_m{}^3(\Delta_{B_l}-1)^2(k_{des}-\Delta_k k) \\ & + 2B_l\Delta_{M_m}M_lM_m{}^2\big(B_m(\Delta_{M_m}+\Delta_{B_m}\Delta_{M_l} \\ & + \Delta_{B_l}\Delta_{M_m}-\Delta_{B_l}\Delta_{B_m}\Delta_{M_l}-2\Delta_k\Delta_{M_m})+D(\Delta_{Mm} \\ & + \Delta_{M_l}+\Delta_{B_l}\Delta_{M_m}-\Delta_{B_l}\Delta_{M_l}-2\Delta_k\Delta_{M_m})\big)(k_{des}-\Delta_k k)\Big)\end{aligned} \tag{23}$$

where $f(u)$ is a function that is positive and increases with u. Qualitatively, (24) highlights that D^4 contributes to the positive part of $N_I(j\omega_m)$, meaning that if it is tuned sufficiently high, the positiveness of $I_\Delta(j\omega)$ is ensured. Conversely, it is necessary to further increase P. Therefore, it is possible to conclude that the parameter errors will not compromise passivity as long as the gains are tuned properly.

5.2 Stability For the closed loop stability it is neces-

sary that all eigenvalues have negative real part. The polynomial characteristic of the new matrix $\boldsymbol{A}_{cl}$ can be derived as:

$$\begin{aligned} Z(s) &= (\Delta_k \Delta_{M_l} {M_l}^2 M_m) z^5 + \Delta_k \Delta_{M_l} M_l (D M_l + B_m M_l \\ &+ B_l M_m) z^4 + \Big(\Delta_k M_l \big(M_m (\Delta_{M_m} k_{des} + \Delta_{M_l} k - \Delta_k \Delta_{M_m} k) \\ &+ \Delta_{M_l} M_l (P + k) + B_l \Delta_{M_l} (D + B_m) \big) \Big) z^3 \\ &+ \big(B_m \Delta_{M_l} M_l (\Delta_{B_m} k_{des} + \Delta_k k - \Delta_k \Delta_{B_m} k) \\ &+ \Delta_{M_l} D M_l k_{des} + B_l \Delta_{M_m} M_m (\Delta_k - \Delta_{B_l})(k_{des} - \Delta_k k) \\ &+ B_l \Delta_k \Delta_{M_l} M_l (P + k) \big) z^2 + \Delta_{M_l} M_l k_{des} (P + \Delta_k k) z \end{aligned} \tag{24}$$

which leads to the following conditions:

$$\begin{cases} P > -k - \frac{B_l}{M_l}(D + B_m) - \frac{M_m}{\Delta_{M_l} M_l} \big(\Delta_{M_l} k \\ \quad + \Delta_{M_m} (k_{des} - \Delta_k k) \big) \\ P > -k - \frac{B_m}{B_l \Delta_k} \big(\Delta_{B_m} k_{des} - \Delta_k k (\Delta_{B_m} - 1) \big) \\ \quad - D \frac{k_{des}}{B_l \Delta_k} - \frac{\Delta_{M_m} M_m}{\Delta_k \Delta_{M_l} M_l} (\Delta_k - \Delta_{B_l})(k_{des} - \Delta_k k) \end{cases} \tag{25}$$

which ensure that the coefficients of z^3 and z^2 are positive, being the only ones that can become negative.
All conditions (21), (25) and P_ω expressed with respect to P mean that it has to be tuned sufficiently high. However, as was shown also with the passivity condition, it is worth remarking that also increasing D has beneficial effects, given that it appears with negative sign in both (25) and P_ω (if $\Delta_{M_m} > \Delta_{M_l}$). Lastly, it is possible to see that the most crucial case for the tuning of P and D is when $k_{des} < \Delta_k k$, since all conditions will increase their minimum value given the presence of a term $(k_{des} - \Delta_k k)$. Since in real applications the control gains cannot be increased at will, these considerations allow to conclude that low stiffness values are the most difficult ones to render with the proposed controller.

6. Simulations

Table 1 SEA parameters. The second column displays the parameters used for the simulations. The third column displays the identified values of the experimental setup.

Parameter	Simulations	Experiments
M_m	1.793 kg	1.879 kg
B_m	2.008 Ns/m	30.099 Ns/m
M_l	0.445 kg	0.4617 kg
B_l	4.933 Ns/m	13.864 N s/m
k	3858 N/m	5299 N/m

Simulations are performed in Matlab Simulink to validate the proposed approach, comparing the performance of all methods in rendering both a pure spring with stiffness $k_{des} = 0.5k$, k, $2k$, (except for the BIC, which is not tested for values greater than the physical spring) and a Voigt model with $k_{des} = 0.5k$, $b_{des} = 0.5B_l$ and $k_{des} = 2k$, $b_{des} = 2B_l$. The parameters used for the SEA model are listed in Tab. 1. All controllers have been discretized with a zero-order holder (sampling time 1 ms). Both position measurements are quantized with step 0.1 µm. The derivative term of the PD controllers and the double derivative in the BIC-AF are filtered by a low-pass filter with cutoff frequency of 100 Hz. The external force is generated by a chirp signal with frequency $f = 0.5\,\text{Hz} - 5.5\,\text{Hz}$ and amplitude 5 N. The experiment lasts 4 s with sweep time 2 s. The load acceleration measurement has a band-limited white noise signal of variance $0.006\,\text{m}^2/\text{s}^4$, which is slightly higher than the one observed with the available MEMS accelerometer. The PD controllers are tuned by trial-and-error to obtain the best performance possible in all cases, as well as the KF. The tests are performed employing the double derivative of the load-side encoder for the BIC-AF case, as stated in the original work, where an additional accelerometer on the load-side is not considered. The proposed method is implemented on the KF estimated variables. The results are quantified by applying a Least-Square method between f_{ext} and x_l, $\dot{x}_l$ $\ddot{x}_l$ across the whole dataset to compute the actual rendered impedance parameters. The error of the retrieved values with respect to the desired ones is computed in percentage and reported in Tab. 2. It is worth noting that the load mass does not represent a parameter to be modified with the proposed approach, therefore $M_{des} = M_l$. The same holds also for the load damping for the pure spring case.

6.1 Pure spring The results are presented through the impedance ellipsoids in Fig. 4, where k_{bic}, k_{af}, k_{seff} indicate the rendered impedance with the BIC, the BIC-AF and the SEFF. In this situation, all methods perform very similarly and display the desired stiffness well, validating the effectiveness of the proposed state-feedback controller. The highest error is $\approx 13\,\%$ performed by the BIC-AF for $k_{des} = 0.5k$, while all other cases have errors below 1 %. Very slight differences are appreciable and are mainly attributed to the tuning of the controller gains, especially concerning the rendered damping and mass. It was observed that both the BIC-AF and the proposed method were also able to display stiffness values higher than those selected, without causing instability. However, these results would be obtained with an input highly affected by noise, which is undesirable in a real experimental setup. Therefore, they are considered unacceptable. Also, it was observed that by reducing the PD gains, the input behavior improves, at the cost of reducing the accuracy of the rendered impedance. A trade-off is therefore necessary according to the application and the available experimental conditions: a more aggressive controller results in better impedance rendering, with a reduced range of allowed stiffness values. The opposite holds for softer control actions.

6.2 Voigt model Tests are also carried out for the Voigt model case, with results illustrated in Fig. 4(b). In all cases, accurate results are obtained for the mass and spring (equal to M_l and k_{des}), but only the proposed method returned damper values within 10 % of b_{des}. The high error of the BIC and BIC-AF is attributed to the need of using the triple derivative of the load position, thus introducing significant noise into the system. Although the results presented appear to be satisfactory with the SEFF, the control actions computed for obtaining them were far from smooth. With all this considered, a Voigt model will not be implemented experimentally and will limit the analysis to the simulated case.

7. Experimental Results

The impedance control schemes considered are tested on a real SEA device, shown in Fig. 6. The setup is composed

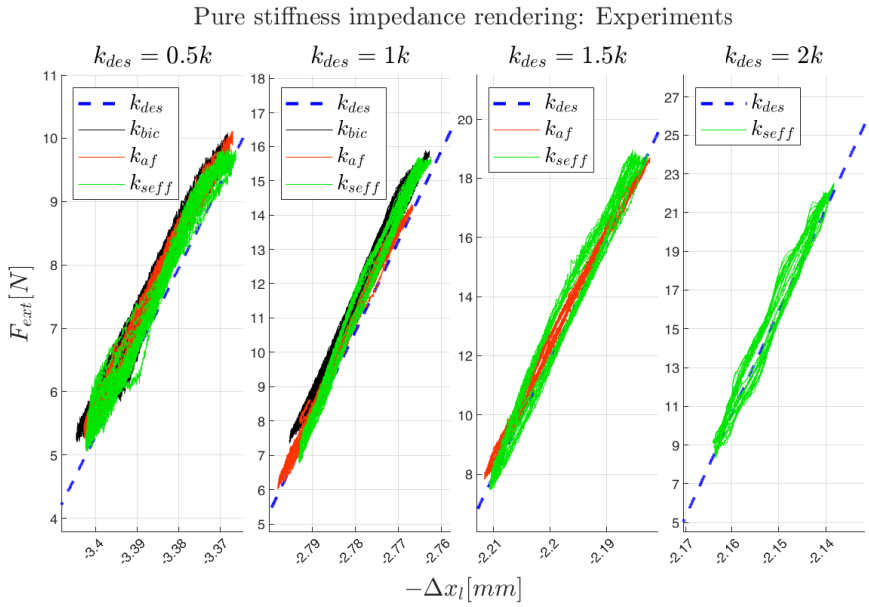

Figure 5 Experimental results for pure spring: $k_{des} = 0.5k,\ k,\ 1.5k,\ 2k$. In all figures, dashed blue line is the desired stiffness, black line refers to BIC, red line refers to BIC-AF and green line refers to SEFF methods.

Table 2 Simulation results of rendered impedance. The numbers reported present the percentage error with respect to k_{des}, b_{des} ans M_l.

	Simulation		
	BIC	BIC-AF	SEFF
$0.5k$	-0.15, 20.5, -0.24	-13.00, -12.84, -0.59	0.60, -17.76, 16.43
k	-0.25, -0.49, -2.84	-0.25, -0.49, -2.84	-0.36, -8.06, -0.95
$2k$		5.97, 26.43, -12.10	-0.62, -14.00, -13.21
$0.5k$, $0.5B_l$	-0.15, 275.38, -1.87	-12.97, 208.74, -2.29	-0.06, -5.38, 7.82
$2k$, $2B_l$		6.03, 98.03, -17.78	0.08, -11.93, -5.81

Table 3 Experimental results of rendered impedance. The numbers reported present the percentage error with respect to k_{des}, b_{des} ans M_l.

	Experiments		
	BIC	BIC-AF	SEFF
$0.5k$	-0.04, -220.65, -10.93	-0.71, 298.56, -8.03	4.07, 99.63, 108.99
k	6.23, -271.78, -14.55	-1.10, 69.52, 222.08	1.14, -377.83, 607.44
$1.5k$		-5.05, 247.60, -10.54	2.03, -88.14, 225.26
$2k$			1.99, -91.43, 49.10

of two linear motors (GMC Hillstone, S160Q and S120Q), one used as actuator and the other as load, mounted in linear ball bearings and connected by a leaf spring. Both masses are equipped with linear encoders (Renishaw RGH24Y, resolution 0.1 µm, and RGH24X, resolution 1 µm, respectively) and two identical MEMS accelerometers (Analog Devices, ADXL335 3-Axis accelerometer, ±3 g, noise variance ≈ 0.0004 and 0.0006 m^2s^{-4}) are mounted on the load slide and on the support of the system. The support-side accelerometer only adds noise to the KF, since gravity is not affecting the

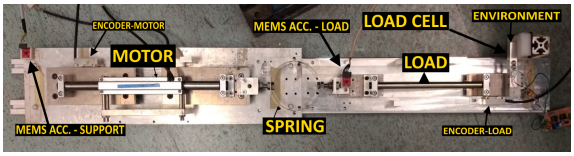

Figure 6 Experimental setup used for experiments.

setup, for a fair comparison between the controllers. The external force is measured by a load cell (HT Sensor Technology, TAL220 Straight Bar, 10 kg of full scale). The experiments are carried out in contact with a soft environment, by commanding the load position to follow a chirp reference signal with frequency $f = 0.2\,\text{Hz} - 3\,\text{Hz}$ and amplitude 3 mm, in 10 s. The identified parameters, obtained from a frequency response function analysis, are listed in Tab. 1. The experiments follow the same rationale as the simulations, with desired stiffness values $k_{des} = 0.5k,\ k,\ 1.5k,\ 2k$. All experiments are run in real time on the Simulink Desktop Real-Time toolbox, with zero-order hold discretized versions of the controllers, sampled at 1 ms. The cutoff frequency of the first and double derivative filters is set to 50 Hz, which was observed to provide the best performance in terms of stability, given the low resolution of the load-side encoder. The results are presented by means of the impedance ellipsoids in Fig. 5, where k_{bic}, k_{af}, k_{seff} indicate the rendered impedance with the relative method. Tab. 3 reports the results obtained with the Least-Square method used to retrieve the actual rendered parameters, as done also in the simulations. However, this approach is highly affected by noise in the real experimental setup, especially considering the absence of the measured load velocity, therefore the values concerning the rendered damping and mass are not informative. This effect is also amplified by the filtering actions on both the PD controllers and the KF, which introduce a delay in the feedback terms that causes a damping variation from the ideal value B_l. However, the stiffness is still reliable.

All controllers are also able in the experimental setup to accurately render the desired stiffness values, with the maximum error of 6 % for the BIC when $k_{des} = k$. All the other cases show errors under 5 %. The major differences can be attributed to modeling errors and control parameters that are quite sensible in the available experimental setup that is affected by some nonlinearities. Considering the maximum

displayable stiffness, it was found that the proposed method is the only one able to reach $k_{des} = 2k$. The BIC-AF scheme cannot reach $k_{des} = 2k$, given the low bandwidth caused by filtering the derivatives.

8. Conclusions

This paper presented a novel impedance control method for SEAs, based on state and external force feedback. The method relies on an MEMS acceleration based-KF for estimating the load-side variables and the external force, not requiring a load position sensor. The proposed approach can be extremely useful in those scenarios where it is difficult to mount encoders on the end effector, and they can be substituted by low-cost and size accelerometers. Acceleration-based solutions in the SEA literature show improved results compared to load encoder-based solutions, further motivating this approach. The proposed controller can render stiffness values greater than the physical spring, guaranteeing passivity. The proposed method performed well in rendering a pure spring, although significant difficulties may arise when a Voigt model is of interest. Future works will consider the analysis of robustness to parametric variations of the proposed scheme, to study the effects on passivity, and further developments towards variable impedance control.

References

(1) Budau Petrea, R., Oboe, R. & Michieletto, G. Safe High Stiffness Impedance Control for Series Elastic Actuators using Collocated Position Feedback. *2022 International Power Electronics Conference (IPEC-Himeji 2022- ECCE Asia)*. pp. 247-254 (2022)

(2) Pratt, G. & Williamson, M. Series elastic actuators. *Proceedings Of 1995 IEEE/RSJ International Conference On Intelligent Robots And Systems*. **1** pp. 399-406 (1995,8)

(3) Mosadeghzad, M., Medrano-Cerda, G., Saglia, J., Tsagarakis, N. & Caldwell, D. Comparison of various active impedance control approaches, modeling, implementation, passivity, stability and trade-offs. *2012 IEEE/ASME International Conference On Advanced Intelligent Mechatronics (AIM)*. pp. 342-348 (2012)

(4) Hogan, N. Impedance control of industrial robots. *Robotics And Computer-Integrated Manufacturing*. **1** pp. 97-113 (2000,1)

(5) Vallery, H., Veneman, J., Asseldonk, E., Ekkelenkamp, R., Buss, M. & Der Kooij, H. Compliant actuation of rehabilitation robots. *IEEE Robotics Automation Magazine*. **15**, 60-69 (2008)

(6) Tagliamonte, N. & Accoto, D. Passivity constraints for the impedance control of series elastic actuators. *Proceedings Of The Institution Of Mechanical Engineers, Part I: Journal Of Systems And Control Engineering*. **228** pp. 138-153 (2013,3)

(7) Tosun, F. & Patoglu, V. Necessary and Sufficient Conditions for the Passivity of Impedance Rendering With Velocity-Sourced Series Elastic Actuation. *IEEE Transactions On Robotics*. **36**, 757-772 (2020)

(8) Li, S., Li, J., Tian, G. & Shang, H. Stiffness Adjustment for a Single-Link Robot Arm Driven by Series Elastic Actuator in Muscle Training. *IEEE Access*. **7** pp. 65029-65039 (2019)

(9) Shardyko, I., Samorodova, M. & Titov, V. Series Elastic Actuator Control Based on Active Damping Injection with Positive Torque Feedback. *2021 International Conference On Industrial Engineering, Applications And Manufacturing (ICIEAM)*. pp. 613-618 (2021)

(10) Lee, H., Lee, J., Ryu, J. & Oh, S. Relaxing the Conservatism of Passivity Condition for Impedance Controlled Series Elastic Actuators. *2019 IEEE/RSJ International Conference On Intelligent Robots And Systems (IROS)*. pp. 7610-7615 (2019)

(11) Calanca, A. & Fiorini, P. Human-Adaptive Control of Series Elastic Actuators. *Robotica*. (2014,12)

(12) Calanca, A. & Fiorini, P. Impedance control of series elastic actuators based on well-defined force dynamics. *Robotics And Autonomous Systems*. **96** (2017,7)

(13) Calanca, A. & Fiorini, P. A Rationale for Acceleration Feedback in Force Control of Series Elastic Actuators. *IEEE Transactions On Robotics*. **34**, 48-61 (2018)

(14) Sensinger, J. & Weir, R. Unconstrained Impedance Control Using a Compact Series Elastic Actuator. *2006 2nd IEEE/ASME International Conference On Mechatronics And Embedded Systems And Applications*. pp. 1-6 (2006)

(15) Boaventura, T. & Buchli, J. Acceleration-based transparency control framework for wearable robots. *2016 IEEE/RSJ International Conference On Intelligent Robots And Systems (IROS)*. pp. 5683-5688 (2016)

(16) De Luca, A., Schroder, D. & Thummel, M. An Acceleration-based State Observer for Robot Manipulators with Elastic Joints. *Proceedings 2007 IEEE International Conference On Robotics And Automation*. pp. 3817-3823 (2007)

(17) Lee, H., Ryu, J., Lee, J. & Oh, S. Passivity Controller Based on Load-Side Damping Assignment for High Stiffness Controlled Series Elastic Actuators. *IEEE Transactions On Industrial Electronics*. **68**, 871-881 (2021)

(18) Calanca, A., Muradore, R. & Fiorini, P. Impedance control of series elastic actuators: Passivity and acceleration-based control. *Mechatronics*. **47** pp. 37-48 (2017,11)

(19) Yokoyama, M., Petrea, R., Oboe, R. & Shimono, T. External Force Estimation in Linear Series Elastic Actuator Without Load-Side Encoder. *IEEE Transactions On Industrial Electronics*. **68**, 861-870 (2021)

(20) Cheon, Dasol, Oh, Sehoon. (2018). Acceleration Based Force Estimation in Series Elastic Actuator. 5062-5067. 10.1109/IECON.2018.8592880.

(21) Nagatsu, Y. & Katsura, S. High-order disturbance estimation using Kalman filter for precise reaction-torque control. *2016 IEEE 14th International Workshop On Advanced Motion Control (AMC)*. pp. 79-84 (2016)

(22) Ferretti, G., Magnani, G. & Rocco, P. Impedance control for elastic joints industrial manipulators. *IEEE Transactions On Robotics And Automation*. **20**, 488-498 (2004)

Razvan Andrei Budau Petrea (Non-member) was born in Bacau, Romania, in 1991. He received the M.S. degree in Automation Engineering and the Ph.D. degree in Mechatronics Engineering from the University of Padova, Padova, Italy, in 2017 and 2022, respectively. He is currently a research grant holder at the Department of Management and Engineering, University of Padova. His research interests include the fields of motion control, interaction force control of collaborative robotics and SEAs, and advanced control systems.

Roberto Oboe (Member) was born in Lonigo, Italy, on October 26, 1963. He received the Laurea degree (cum laude) in electrical engineering and the Ph.D. degree from the University of Padova, Padova, Italy, in 1988 and 1992, respectively. He is presently Associate Professor of Automatic Control at the Department of Management and Engineering of the University of Padova, Vicenza, Italy. His research interests are in the fields of applied digital control, telerobotics, haptic devices, rehabilitation robots and applications and control of MEMS.

Giulia Michieletto (Non-member) received the M.S. degree in Automation Engineering and the Ph.D. degree in Information Engineering from the University of Padova, Padova, Italy, in 2014 and 2018. She is currently an Assistant Professor with the Department of Management and Engineering, University of Padova. From March 2016 to February 2017, she was a Visiting Researcher with LAAS-CNRS, Toulouse, France. From February 2018 to November 2019, she was a Postdoc Fellow with the SPARCS group, at University of Padova, Italy. Her principal research interests include the modeling, control, and experimental validation of ground and aerial autonomous vehicles acting either as a single unit or within a cooperative multi-agent context.